Comparative analysis of global hand appearance-based person recognition

Helin Dutağacı
Bülent Sankur
Boğaziçi University
Department of Electrical-Electronics Engineering
Bebek, Istanbul, Turkey
E-mail: dutagach@boun.edu.tr

Erdem Yörük
Johns Hopkins University
Center for Imaging Science
3400 North Charles Street, 307-B Clark Hall
Baltimore, Maryland 21218

Abstract. *We provide a survey of hand biometric techniques in the literature and incorporate several novel results of hand-based personal identification and verification. We compare several feature sets in the shape-only and shape-plus-texture categories, emphasizing the relevance of a proper hand normalization scheme in the success of any biometric scheme. The preference of the left and right hands or of ambidextrous access control is explored. Since the business case of a biometric device partly hinges on the longevity of its features and the generalization ability of its database, we have tested our scheme with time-lapse data as well as with subjects that were unseen during the training stage. Our experiments were conducted on a hand database that is an order of magnitude larger than any existing one in the literature. © 2008 SPIE and IS&T.*
[DOI: 10.1117/1.2890986]

1 Introduction

Hand recognition systems are among the oldest biometric tools for automatic person authentication. Access control devices have been manufactured and commercialized since the late 1970s. Several patents have already been issued for hand recognition devices,[1–5] and live applications have been launched and used at nuclear plants, airports, and hotels in the last 30 years.[6,7] The first biometric device was manufactured in 1971, and it was indeed a hand-based recognition tool called Identimat.[1] Hundreds of Identimat devices were used for security purposes at the Department of Energy, U.S. Naval Intelligence in the 1970s. However, hand biometry has gained interest in academic circles, mostly with the progress of computer vision research, only in the last decade. Before 1998, the publications were limited to patents and two special reports.[6,8] Figure 1 gives the increase in the number of publications since 1998.

Hand-based person recognition is reliable, low-cost, and user-friendly, all in all, a viable solution for a range of access control applications. Other "nearest competitor" modalities are face, iris, fingerprint, and retinal biometry. The face recognition alternative is another low-cost solution for access control. However, unless several challenging issues are satisfactorily solved, such as illumination, pose, and facial expression variations and occlusions due to accessories, it will be limited to controlled niche applications. Unsupervised face recognition, where the user does not have to pose for the camera, requires both detection and segmentation of the facial region from cluttered backgrounds and normalization of the face, both challenging problems. Despite its attraction, automatic face recognition within its current state of art is regarded as a biometric modality with inadequate reliability.

The iris and retinal modalities demand specialized acquisition devices. Furthermore, due to their intrusive nature, most people feel uncomfortable, and so these modalities will not, in all likelihood, be widely deployed.

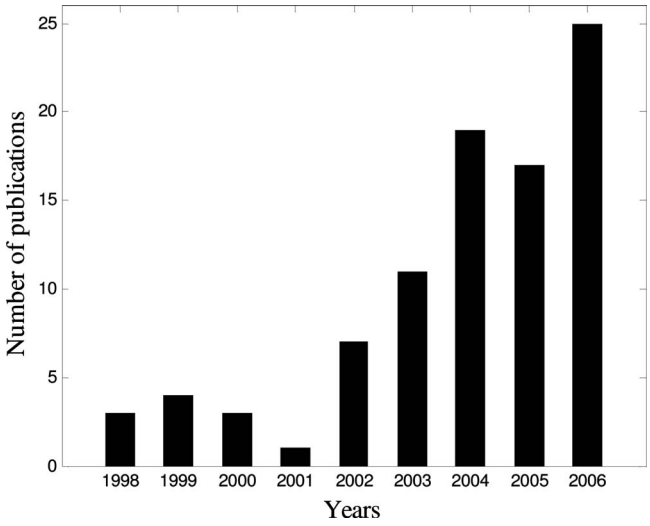

Fig. 1 The progress of hand biometry publications over the years.

Paper 07111SSR received Jun. 16, 2007; revised manuscript received Oct. 17, 2007; accepted for publication Nov. 6, 2007; published online Mar. 21, 2008.
1017-9909/2008/17(1)/011018/19/$25.00 © 2008 SPIE and IS&T.

Fingerprint modality is by far the most studied case, commonly used from forensic evidence collection to personal device access, home access, or Internet access. However, minutiae are very sensitive to cuts and wounds in the finger; hence, fingerprint features from manual laborers or elderly people become less reliable and more difficult to acquire. In fact, up to 4% of the population may fail to provide fingerprints with acceptable quality.[9] Most people still have a certain reticence with fingerprints; for example, fingerprints are considered private by some users, who may not yield fingerprints for commercial applications. There has also been a considerable amount of research on voice authentication, especially in telephone applications. However, speech data suffer from intrapersonal variations due to mood, emotion, illness, and aging. Due to these handicaps, its reliability is low, and so voice-based authentication is not yet a competitor to fingerprint or hand.

In contrast to these techniques, hand biometry offers some advantages. First, data acquisition is economical via commercial low-resolution scanners or cameras, and its processing is relatively simple. Second, according to two public surveys,[8,10] people like hand-based access systems, as they do not consider hand information to be as private as iris or fingerprint in daily applications; hence, they find hand biometry less invasive and more convenient to use than other biometric modalities. Third, hand-based access systems are very suitable for indoor and outdoor usage and can work well in extreme weather and illumination conditions.[8,10] Fourth, the hand features of adults are more stable over time and are not susceptible to major changes, except for injury- or arthritis-based deformations. Finally, hand-based biometric information has been shown to be very reliable[11,12] and can successfully recognize people among populations of the order of several hundreds. We conjecture, therefore, that the time has come to deploy hand biometric devices for daily applications ranging from access to hospitals, child daycare centers, industrial plants, and universities to more challenging situations at border control and airports. They can also be used to enhance the security of e-commerce and banking applications via integration to the conventional systems using PIN codes and passwords.

This paper has the dual purpose of providing a literature survey on hand biometry and of presenting novel performance results. Our basic algorithm was elaborated on our previous work.[11,12] In this respect, we consider the generalization ability of our ICA-based feature extraction algorithm from small to large populations, the preference for right or left hand, the advantage of ambidextrous testing, the performance of new features, and various fusion schemes to improve the performance. In addition to the analysis of our global hand appearance-based approach, we provide comparative performance results of various techniques on a large database consisting of 918 subjects. Some of these techniques were previously applied on hands for personal recognition; others are considered first in this paper as tools of characterizing human hands, such as the principal component analysis of global hand appearance and Fourier descriptors of hand contour.

In Section 2, we introduce the characteristics of the hand and briefly survey the existing features and algorithms. In Section 3, we discuss the published hand acquisition setups. In Section 4, we describe our normalization scheme along with its preprocessing stage. In Section 5, we present hand features that we have tested for person recognition in this work. Section 6 gives the experimental results, and finally we conclude in Section 7.

2 Characteristics of the Human Hand

In this section, we describe the characteristics of the human hand and its aspects relevant for feature extraction.

2.1 *The Skeleton of the Hand*

The anatomic structure and biomechanics of the human hand have interested researchers working in the areas of computer animation, hand gesture, and sign language recognition. This information is also beneficial for hand biometry.

The hand contains 27 bones, categorized into three groups: the carpals in the wrist, the metacarpal bones that run along the palm, and the phalanx bones in the fingers.[13] Figure 2 shows the skeletal model of the human hand. When laid on a flat surface, the interphalangeal joints at the fingers become fixed since the extension and flexion of the fingers are disabled. However, those of the thumb can still move slightly since they are not totally in the supine position. The carpal-metacarpal joints are already limited in their freedom of movement, again except for the thumb. Thus, a hand lying on a flat surface is reduced to seven degrees of freedom; three at the three joints of the thumb, and four at the metacarpal-phalanx joints of the four fingers. The metacarpal-phalanx joints (MCP) are the pivots where the fingers make adduction/abduction movements, i.e., lateral movements on the plane. The orientation of the thumb, on the other hand, is controlled by its carpal-metacarpal joint (TM in Fig. 2) and the thumb shows relatively high in-plane flexibility.

Kuch and Huang[14] used a set of constraints on finger movements for gesture modeling where the range of in-plane rotation angles of the four fingers around their pivot (MCP joints) is taken between −15 deg and 15 deg. A more complex set of relations was assumed between the in-plane angles of the three joints of the thumb. Lin *et al.*[15] developed another hand-skeleton model under similar assumptions, with the additional constraint of a rigid middle finger. In our hand-posture normalization scheme,[11,12] we make use of the five degrees-of-freedom model, so that we rotate the fingers to preset reference angles based on an estimate of their metacarpal pivot locations.[12] The posture normalization algorithm is described briefly in Section 4 and in more detail in our previous work.[12]

2.2 *The Geometry of the Hand*

Geometrical measures have been used in most patented methods of hand-based identification and in earlier publications. Ernst[2] mentioned the anthropological studies that stated that the length and breadth of the hand had very little statistical correlation. Since both sizes were useful measures, he developed a string-based, mechanical aperture to measure the width and the length of the hand. Miller advanced this scheme with an electro-mechanical system, called Identimation, that measured the lengths of the four fingers and compared them with measurements prerecorded on an identification card.[1] In 1972, Jacoby *et al.* came up

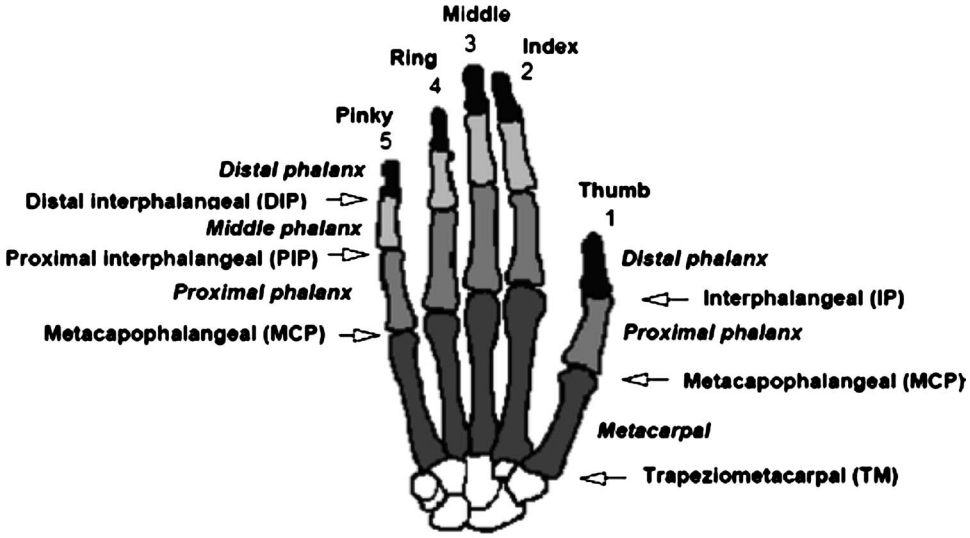

Fig. 2 The skeleton of the hand (from Ref. 13).

with the first optical system that measured the distances between fingertips and finger crotches through a scanner.[3]

Geometrical features of the hand, also referred to as "hand dimensions" in the literature, constitute the bulk of the hand features adopted in most hand recognition systems. One advantage is that geometrical features are more or less invariant to the global positioning of the hand and to the individual planar orientations of the fingers. Among numerous geometrical measures, we can cite the lengths, widths, areas, and perimeters of the hand, fingers, and the palm. Jain *et al.* have come to the conclusion that hand geometrical features solely are not sufficiently discriminative.[16] This is due to the facts that they are somewhat correlated and that there are at most 50 geometrical features. For the present state of the art, they are not viewed as suitable for identification (one-to-many comparison) purposes, but instead can be used for verification (one-to-one comparison) tasks.[16] Therefore, for more demanding applications, one must revert to alternative features such as hand global shape, appearance, and/or texture.

Hand geometrical features consist of a set of measured dimensions, such as the lengths, widths, and areas of the fingers, the hand, and the palm. Jain *et al.* used 16 axes predetermined with the aid of five pegs.[16] The gray-level profiles along these axes are modeled as an ideal profile contaminated by Gaussian noise. Using this profile model, 15 geometrical features are extracted and tested for verification. In their peg-aided identification system, Sanchez-Reillo *et al.* used a similar set of geometric features, containing the widths of the four fingers measured at different latitudes, the lengths of the three fingers and the palm.[17] The distances among three interfinger points (finger valleys) and the angles between the lines connecting these points are also part of the set. Wong and Shi, in addition to finger widths, lengths, and interfinger baselines, employed the fingertip regions.[18] The fingertip regions correspond to the top one-eighth portion of the index, middle, and ring fingers. The curves extracted from these fingertip regions are then aligned, resampled, and compared via the Euclidean distance. Bulatov *et al.* described a peg-free system where 30 geometrical measures are extracted from the hand images.[19] In addition to the widths, perimeters, and areas of the fingers, they also incorporated the radii of inscribing circles of the fingers and the radius of the largest inscribing circle of the palm. However, they did not give any information on the extraction procedure of these features.

While geometrical features are simple to extract, they have certain disadvantages. First, they are not discriminating enough to be used in identification tasks and in high-security verification scenarios. The reason is that this approach reduces the holistic shape information to a small set of features, and obviously texture cannot be exploited. Furthermore, a simple set of geometrical measures can be more easily faked or compromised. For these reasons, some authors propose the fusion of geometry-based features with other characteristics of the hand such as the finger shapes[20] or the palmprint features.[21–23]

2.3 *The Shape of the Hand*

The shape or the silhouette of the hand has gained little attention in the literature for person identification despite considerable literature on shape matching in computer vision. Jain and Duta were the first to propose deformable shape analysis and to develop an algorithm where hand silhouettes are registered and compared in terms of the mean alignment error.[24]

The hand shape, surprisingly, exhibits great variation among individuals. The silhouettes contain much richer information than geometrical measures of the hand. For example, the roundness of fingertips, the shape of the thumb, the sharpness of finger valleys, etc. are not necessarily incorporated in the geometric measurements. The geometrical features, no matter how detailed, are surpassed by the shape features in parts-based or holistic analysis.

The major roadblock for the use of the hand shape as a person identifier has been the fact that the hand is a highly deformable and articulated organ, making it challenging to characterize the global shape. The intrapersonal variability of the hand shape, if not properly normalized, can be much

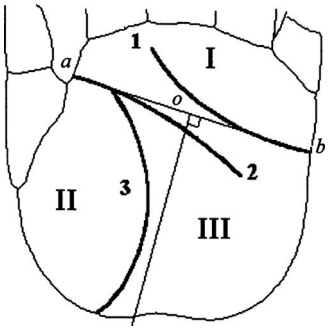

Fig. 3 Principal lines (1: heart line, 2: head line, 3: life line) (from Ref. 30).

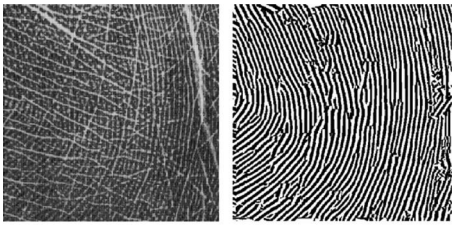

Fig. 4 (a) Creases are the irregular lines. Ridges are the regular lines flowing from top to bottom. (b) Ridges after elimination of the creases (from Ref. 37).

bigger than the interpersonal differences. Thus, researchers often use pegs to fix the position of the hand and the orientation of the fingers.[24] Konukoğlu *et al.*[11] and Yörük *et al.*[12] developed a detailed hand normalization algorithm, where hands are brought to a normalized posture from any uncontrolled positioning. Konukoğlu *et al.* experimented with various shape features; for example, they used a modified Hausdorff distance for hand contours and independent component analysis (ICA) features of the binary hands.[11] Of the two ICA architectures, the recognition performance of the ICA2 architecture was found to be superior to the ICA1 architecture. Yörük *et al.* conducted experiments with alternative shape features such as active shape models,[25] angular radial transform,[26] and distance transform.[27] For the active shape model approach, the set of 2D coordinates of the contour points is reorganized according to the 11 fiduciary reference points, namely 5 fingertips, 4 finger crotches, and 2 palm terminations. The contours are then resampled in order to guarantee correspondence between contour elements of all hands.

2.4 *The Palm of the Hand*

Perhaps inspired by the recent advances in fingerprint analysis, the palm has attracted a lot of attention in the last decade. The palm exhibits a rich pattern of striations that are believed to be unique to each individual. In fact, palmprints have been utilized as person identifiers for more than 100 years. These techniques, however, were not automated and required the application of ink, powders, or other chemicals to put ridges into evidence. Notice that the ridgeology practice encompasses not only palms but also footprints and any other striated surface.[28] The use of palmprint features for computer-based identification was first proposed by Shu and Zhang in 1998.[29] Later Zhang and colleagues developed a series of computer vision algorithms for processing palmprint features.

Palmprint features can be divided into three categories based on their scale: (1) palm lines including the principal lines; (2) creases or wrinkles, and (3) ridges or the minutiae. The palm lines and the principal palm lines (Fig. 3) are discriminating features that are considered to be stable over time.[30] Creases or wrinkles are irregular lines that are thinner than the principal lines [Fig. 4(a)], and ridges correspond to regular and very thin lines that are similar to the minutiae of the fingerprints [Fig. 4(b)]. The extraction of the minutiae requires high-resolution imaging and the elimination of palm lines and creases. The minutiae of the palmprint are as reliable for identification as those of the fingerprint and have been used for forensic applications.[28]

Shu and Zhang were the first to publish on palmprint-based person recognition.[29,30] They applied nonlinear filters to detect the principal palm lines and encoded the detected lines by their endpoints and midpoints. Duta *et al.* used a set of feature points along the prominent palm lines and the associated line orientations to match two palmprint images.[31] They did not explicitly extract palm lines as Shu and Zhang[30] and Liu and Zhang[32] did, but used only isolated points along palm lines. Wu *et al.* proposed a two-stage palm line extraction scheme.[33] In the first stage, morphological operators are applied to the palm image to extract palm lines in different directions. In the second stage, a recursive process is used to trace and complete the palm line using the local information along the regions extracted in the first stage. You *et al.* proposed a hierarchical palm-matching algorithm[34] where global texture energy obtained by Laws' convolution masks[35] were used to select a small number of candidate palms at a coarse level. An interest point-based matching algorithm was applied to the candidate palms at a fine level to achieve the final decision. The interest points along the palm lines are similar to the feature points of Duta *et al.*[31] and are detected by local operators.

Palmprints have a large number of creases, which are assumed to be stable in a person's life.[36] Chen *et al.* tried to detect the creases by using a direction computing method based on the local gray-level values.[36] Funada *et al.* suggested the use of ridges for palmprint characterization.[37] The ridge patterns, such as the termination of bifurcations, i.e., minutiae, are inherited from the fingerprint literature. However, the palmprint minutiae are crossed by many creases (Fig. 4). Funada *et al.* set out first to eliminate these creases[37] and then to extract ridge candidates by fitting the local image to a ridge model. A ridge pattern is approximated by a two-dimensional sine wave, and the pairs of peaks are detected in the power spectrum of the local image.

In general, the palmprint features, such as principal lines, creases, wrinkles, delta points, minutiae, etc., are difficult to extract and characterize, especially in low-resolution images. Researchers have often used ink to enhance these line structures of the palm.[29,30,34,36] Alternatively, instead of explicitly extracting and coding the palm lines, creases, and interest points, edge maps can be used directly to compare palm images. The edge maps

provide global information, even at low resolutions, about the magnitudes and directions of the palm lines and creases. Wu *et al.* used a fuzzy directional element energy feature, which provides line structural information about palmprints via encoding the directions and energies of the edges.[38] They proposed a similar notion in one of their recent papers,[39] where they used directional line detectors to obtain a set of line magnitude images. Then these directional images were divided into overlapping grids and directional line energy features were computed. Han *et al.* applied Sobel and morphological operators to the central part of the palm image and used the mean values of the grid cells as features.[40] Similarly, Kumar *et al.* used line detection operators consisting of four orientation-convolution masks.[21,22] The output of these operators is merged in one single directional map, and the standard deviations of pixels of overlapping blocks on the directional map are used as the palmprint features.

Li *et al.* proposed the use of the Hausdorff distance to compare the line edge maps of two palm images.[41] The lines and curves, forming an edge map, are compared by the line segment Hausdorff distance and the curve segment Hausdorff distance.

An alternative way is to consider the central part of the palm as a textured image and apply well-known pattern recognition techniques to represent the palm region. These techniques include Gabor filters,[42–45] Global texture energy,[34] the Fourier transform,[23,46–48] eigenpalms through the Karhunen–Loeve transform,[48–51] Fishers' linear discriminant,[50,51] Zernike moment invariants,[52] wavelets,[50,53–55] independent component analysis,[50,56,57] the correlation filter classifier,[58] Haar wavelets,[59] global and local texture energy,[60,61] and Hu moment invariants.[62]

2.5 *The Fingers*

Since the shape of the hand is characterized by great intraperson variation due to the articulation of fingers, some authors segment the hand into its fingers in order to separately model the shapes of the individual fingers.[20,63,64]

Oden *et al.* proposed modeling the shape of each individual finger with implicit fourth-degree polynomial functions.[20] Then the Keren invariants are extracted from the fitted polynomials to be used as features invariant to affine transformations.[65] However, they experimented on an insufficiently small data set. Xiong *et al.* separated and identified multiple rigid fingers under Euclidean transformations.[63] The fingers are aligned with the aid of an elliptical model, and their similarity is measured on finger widths observed at predefined nodes. Fouquier *et al.* proposed a method based on the projection of finger boundaries on the major axis of the fingers.[66] They segmented the fingers using fingertips and interfinger valleys, and computed the histogram of the distances from the finger boundary to the major axis of each finger. The histograms, smoothed with a Gaussian kernel, constitute their feature vectors.

The inner side of fingers is textured with creases, whose location and pattern differ from person to person. Joshi *et al.* proposed using the gray-level values of the finger images for person verification.[67] They defined a feature called the *wide line integrated profile* (WNIL), which is obtained by averaging the gray-level values over 5-mm-wide bands. The distinct peaks in the line profile correspond to the creases of the fingers. Two profiles are then matched by choosing the maximum of the correlation values calculated in a range of shift values. Since this scheme necessitates precise localization and alignment of fingers, the authors used a special acquisition setup consisting of a mechanical guide and a micro switch to get an already-aligned finger image from the user. The system acquires one finger at a time, a constraint that decreases the user-friendliness of the system, especially if multiple fingers are to be matched. Ribaric and Fratric proposed an eigenfinger approach, which is then fused with either eigenpalms[68] or finger geometry.[69] They extracted strip-like finger subimages and applied the Karhunen–Loeve transform to obtain eigenfingers. These eigenfingers encode the texture variation among the fingers of the database.

2.6 *Joint Hand Shape and Texture Features*

Palmprint and hand shape information provides independent biometric identity features; hence, one can benefit from their joint use for person recognition. The integration of palmprint and shape is generally performed at the feature level by using palmprint features and simple geometrical measures together or at the score or decision level by constructing classifiers guided by palmprint and shape-based experts.[22]

Kumar *et al.* fused the palmprint features and geometrical measures at both the feature level and the score level.[22] In order to characterize the palm, they used line detection operators consisting of convolution masks, each of which is tuned to one of the four orientations. The output of these operators is merged in one single directional map, and standard deviations of pixels of overlapping blocks on the directional map are used as the palmprint features. Eighteen geometrical measures such as widths and lengths of the fingers and the palm are estimated to represent the shape. The palmprint and geometrical features are concatenated to form a single feature vector representing the hand. In addition to the feature-level fusion scheme, these authors also proposed fusion at the score level, where individual matching scores for palmprint and hand geometry are combined using the max rule.

3 Hand Image Acquisition

3.1 *Acquisition Devices*

After the first electromechanical devices focused on geometric features,[1,2] the development of optical and infrared imaging technology made it possible to process hand images with computer vision tools. The Handkey device is a prototypical commercial product of Schlage Recognition Systems (Fig. 5). The device originates from the invention of Sidlauskas, who patented his scanning device in 1988.[4,7] The user positions his or her right hand horizontally between a set of pins that restricts the orientation of the fingers. The image of the hand is acquired by a CCD camera from above and, with the help of a mirror, from the side. Other research groups developed their acquisition setups mostly inspired from the invention of Sidlauskas.[16,17] This setup is suitable for extraction of hand shape, but it does not enable palmprint acquisition.

For systems based on palmprints, the imaging quality is more important. In early work, researchers used ink to get a

(a) (b)

Fig. 5 (a) Handkey II, (b) ID3D Handkey, the commercial hand geometry-based verification devices from Schlage Recognition Systems.

palmprint on the paper, which was then digitized.[29,30,34,36] This laborious technique is only feasible for very specific applications such as criminal identification. High-quality palm images demand contactless design and good illumination. Zhang and colleagues were the first to develop such an acquisition device.[43,46,70] This device, illustrated in Fig. 6 in exploded view, includes a ring-shaped source providing white fluorescent light, a platform with pegs to guide the users, a CCD camera, lens, frame grabber, and A/D converter. It is intended for civilian applications such as access systems and ATMs.

While the device developed by Zhang *et al.*[43,46,70] only acquired palm images, Kumar *et al.* collected data with a setup that can jointly acquire hand shape and palm image (Fig. 6).[21,22] Their device, however, necessitates an uncomfortable positioning of the user's hand facing upwards (Fig. 7). Furthermore, due to the curved nature of the back of the hand, the placement is not unique, which causes some yaw distortion in the hand.

Wong *et al.* discuss the choice between a camera and a scanner for joint hand and palmprint imaging.[70] The camera is advantageous both due to its acquisition speed and because it enables a noncontact setup (Figs. 6 and 7). The

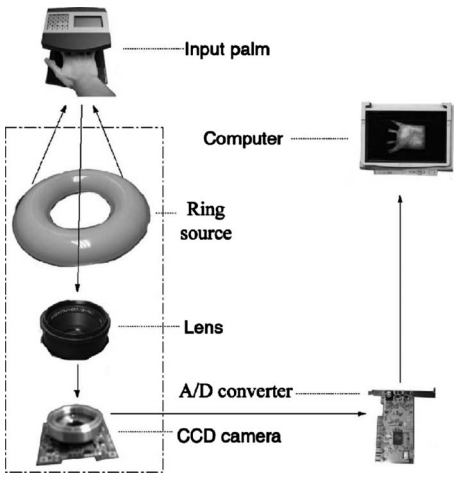

Fig. 6 Palmprint capture device (from Ref. 43).

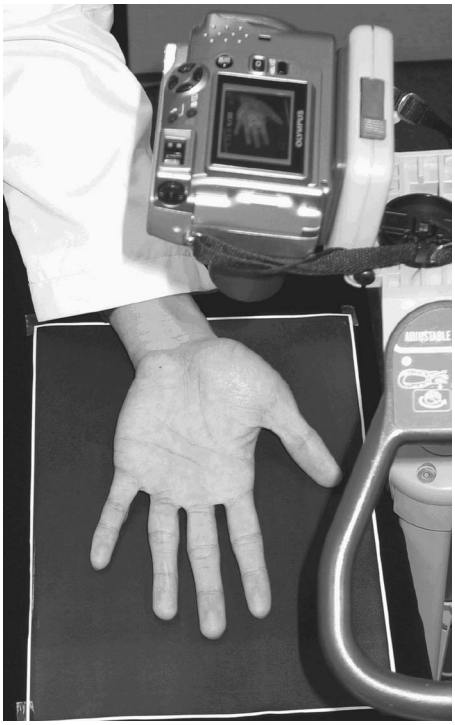

Fig. 7 Hand shape and palm acquisition device of Kumar *et al.* (from Refs. 21 and 22).

hand contact with the scanner's surface deforms the palmprint features according to the pressure level; and the scanner surface should be regularly cleaned up.

Flatbed scanners, on the other hand, provide a viable alternative where the user can comfortably lay his hand, and the resulting image is high-quality with homogeneous dark background and constant illumination. Notice that to achieve conditions similar to those of a scanner, the camera setup should be fixed and focused on the hand, there should be a flat surface for the user to place her hand, and in many cases special illumination is needed. For Web-based access systems, e-commerce, and e-banking applications, special hand or palmprint acquisition devices may not be affordable in home and office environments. Instead, the ubiquitous flatbed scanner is the most appropriate capture device. Many researchers have worked with hand and/or palmprint images acquired by flatbed scanners due to their simplicity and ease of data collection.[11,12,18,19,31,40,47,50,62,68]

Early hand acquisition devices used pegs controlling the finger orientations, thus intending to constrain degrees of freedom for hand articulation.[16,17,24,43,55,67] Presently, peg usage for constraining the position of the fingers is considered to be inappropriate for two reasons: first, it decreases the comfort or user-friendliness of the device due to the training stage to learn proper placement. Second, people whose hands are too small or too big may cause stress deformations especially in the inter-finger valleys due to hard contacts. The new trend is definitely to design peg-free systems.[11,12,18–23,68] These unconstrained acquisition systems rely on posture-independent features or preprocess hand images for posture normalization.

3.2 *Which Hand to Acquire?*

It might seem that the choice between the right and left hand would be inconsequential for hand biometry. For example, since the majority of people are right-handed, it would be a matter of convenience to design right-handed devices. However, some authors have observed a performance differential between right and left hands. For example, Kumar and Shen[47] and Kumar and Zhang[71] have reported that the performance differentials are of the order of 0.5 to 1%. We conjecture that the statistical difference between the right and left hands could be due to the fact that the working hand, often the right one, is plumper and its palm gets deformed more easily with device contact. Similar observations were made over time-lapse images: the intravariations of the right hand are comparatively greater over time.

In many studies,[38,42–45,49,50,59,60] the left and right hand palms of the same person were considered independently, hence as if belonging to different classes, and the performance measurements were done accordingly. In fact, the palmprints and the geometry of the right and left hands of the same person are highly correlated, and the correlation between these two hands can be more advantageously exploited. In our previous work,[12] we showed that the intrapersonal feature distances between left and right hands were much smaller than the interpersonal distances between hands of different people.

One way to utilize the correlated information in the two hands is to apply fusion schemes. For example, Kumar and Zhang[71] used fusion of left and right palmprints with the sum rule at score level. In Section 6.3, we discuss various fusion schemes at the data level, feature level, and score level.

4 Image Processing

In this section, we describe our novel hand normalization algorithm and discuss the relevant work in the literature. When no positioning aids such as fixation pegs are used, hand images exhibit great intraclass variations due to hand placement (rotation and translation) and free finger orientations. With our normalization algorithm, we minimize posture variations and also correct for illumination variations due to the pressure of the hand on the scanner.

4.1 *Segmentation of the Hand from the Background*

For the hand placed on a platen of the acquisition device or on a scanner, the background is almost uniform and therefore segmentation becomes a relatively easy task. In some systems,[16] hand segmentation is not even required, since the hand features are computed directly based on the peg template (Fig. 8).

Jain and Duta used the mean-shift unsupervised segmentation and a contour-following algorithm to extract the shape of the hand.[24] In most other works,[7,18,21,68] simple thresholding is used for segmentation. For example, Kumar *et al.* used Otsu's threshold method.[21] However, segmentation performed with simple thresholding is sensitive to many factors, such as accessories (rings, bracelets, watches) and sleeves, dirt artifacts, and darker skin regions on the hand. The failure to correctly segment and extract the silhouette of the hand causes performance degradation as well as frequent rejection of the authorized users. An-

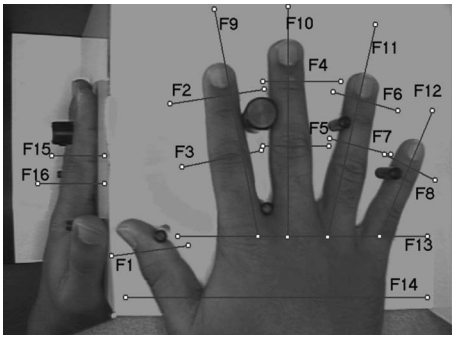

Fig. 8 The axes along which feature values are computed in the algorithm of Jain *et al.* (from Ref. 16).

other important factor is the "portability" of the segmentation algorithm, i.e., the algorithm should be easily adapted to a new setup, with different imaging devices and environmental factors.

We designed a peg-free segmentation and normalization algorithm that operates with a large range of imaging devices, under varying illumination conditions and in the presence of hand accessories and sleeves. We impose only two requirements: (1) the background should be relatively homogeneous; (2) fingers should not touch each other. Figures 9(a)–9(c) show hand images acquired with scanners, cameras, and low-resolution webcams, respectively, and the outcomes of our segmentation and normalization algorithm. The outcome quality of the segmentation and normalization algorithms is independent of imaging devices (scanner or camera) and of any special setup (special illumination, peg usage, etc.).

Figure 12 shows the block diagram of our novel hand normalization scheme along with the illustrative outputs of the intermediate steps. It involves the steps to segment the hand region via K-means clustering, morphological correction, and ring or bandage artifact removal. Morphological operators mop up the holes in the foreground and debris in the background. The presence of rings or bandages on the

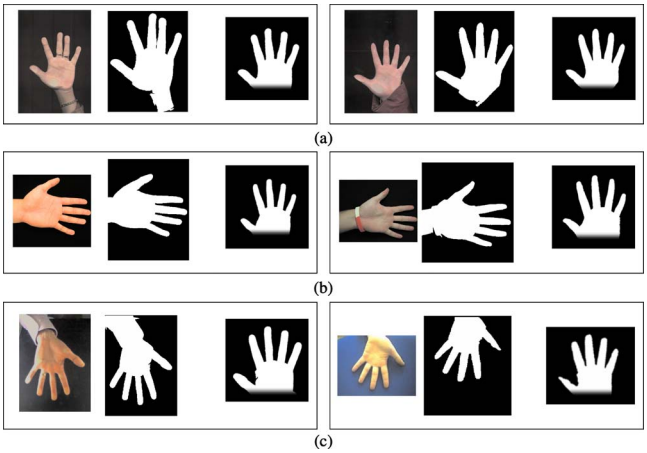

Fig. 9 Results of our segmentation and normalization algorithm for the original hand images of six different persons acquired from (a) two different scanners, (b) two different cameras, and (c) two different low-resolution webcams. First column: acquired image; second column: binarized hand; third column: normalized hand.

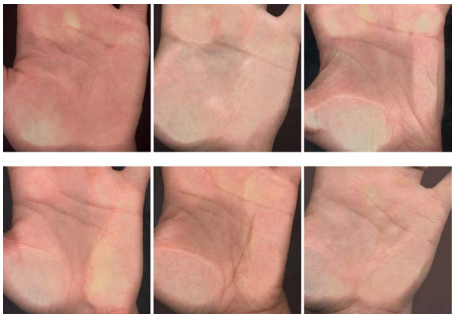

Fig. 10 Palm images where datum points cannot be determined precisely.

finger is detected, and the silhouette is corrected with an "artifact removal" algorithm.[11,12] Finally, the hand and fingers are aligned to fixed orientations.

4.2 *Hand Normalization*

For hand biometry algorithms that utilize nonlocal features, hand normalization is the most critical step. Hand normalization implies positioning of the global hand and orienting the fingers to fixed positions.

Jain and Duta separately aligned pairs of corresponding fingers between the probe and gallery hand using a quasi-exhaustive polynomial search.[24] Using the correspondences obtained from the finger alignment search, they applied Procrustes analysis and declared the mean alignment error as a measure of the distance between two hands. Wong and Shi implemented an alignment algorithm using nine landmarks (fingertips and valleys), which in turn are detected with the extrema of the hand contour curvature.[18] The middle-finger baseline is obtained by the straight line connecting the two valleys around the middle finger. The palm is rotated to a common reference frame according to an axis formed on the middle finger. Then the other fingers are rotated to align with those of a template hand, with matching middle fingers. Kumar *et al.* approximated the binarized shape of the hand by an ellipse.[21,22] They used moments of the binary hand to extract the best-fitting ellipse. The hand is rotated according to the angle of the major axis of this ellipse. This aligned silhouette is then used to compute geometrical measures of the hand and to localize the palmprint region.

The alignment of purely palmprint-based schemes is somewhat different. For example, Zhang and Shu claimed that the three datum points are rotation-invariant and can be used to construct a local coordinate system for the alignment of line features.[30] These references are the endpoints of the heart line and the head line while intersecting with the sides of the palm and their midpoint (points a, b, and o, respectively, in Fig. 3). Obviously, this alignment algorithm is not robust since the assumptions that the life and head lines extend to one side of the palm and that life and head lines merge before ending on the side of the palm do not hold for a nonnegligible portion of the population (Fig. 10). The authors report that this alignment scheme failed in 5% of the images.

Zhang *et al.* proposed a more robust palm extraction and alignment algorithm based on the finger valleys.[43–46,61] Once the two finger valleys, between the index and middle

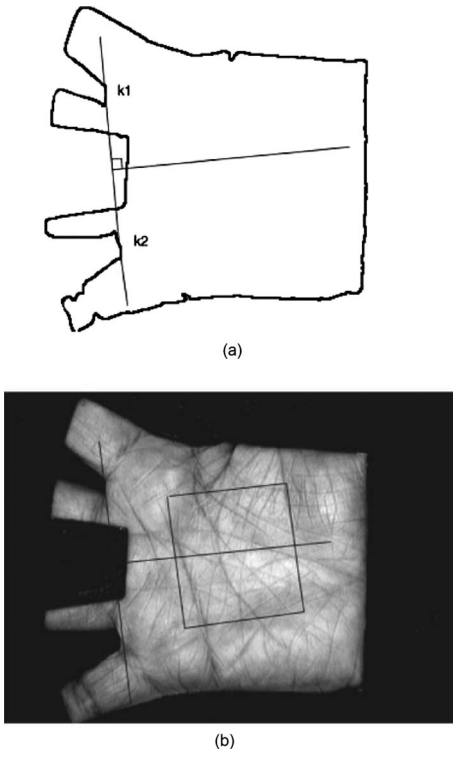

Fig. 11 The palmprint alignment algorithm of Zhang *et al.* (from Ref. 43). (a) The palmprint coordinate system; (b) cropping of the region of interest.

fingers and between the ring and pinky fingers, are detected, the line connecting these two crotches constitutes the y-axis of the palmprint coordinate system. The midpoint corresponds to the origin and the perpendicular line through the midpoint is used as the x-axis [Fig. 11(a)]. The palm image's local coordinate system is rotated to align with a reference coordinate system, and a central subimage is cropped as the aligned palm region of interest [Fig. 11(b)].

Our hand normalization algorithm[11,12] minimizes intra-person variability of the hand postures, finger orientations, and illumination, as illustrated in Fig. 12. Briefly, the hand is translated and rotated to a reference frame, illumination correction is performed on it, and the fingers are rotated around the pivot locations to preset orientations. The details of the normalization procedure can be found in our previous work.[12] The key points and the superiorities of the algorithm can be listed as follows:

- *Robustness to hand accessories*: Users are not obliged to remove their accessories, such as rings, clocks, or bracelets, in this hand-based access system. The segmentation procedure of our normalization algorithm includes a ring and other artifact (like bandage) removal stage.
- *Texture correction*: Any nonuniform illumination effects and discolorations due to pressure applied by the user are corrected. First, the hand texture is converted to gray-level by choosing the principal component color with the largest variance. Second, the artifacts due to the nonuniform pressure are removed by a Gaussian kernel high-pass filtering.
- *Finger rotation around pivots and texture blending*:

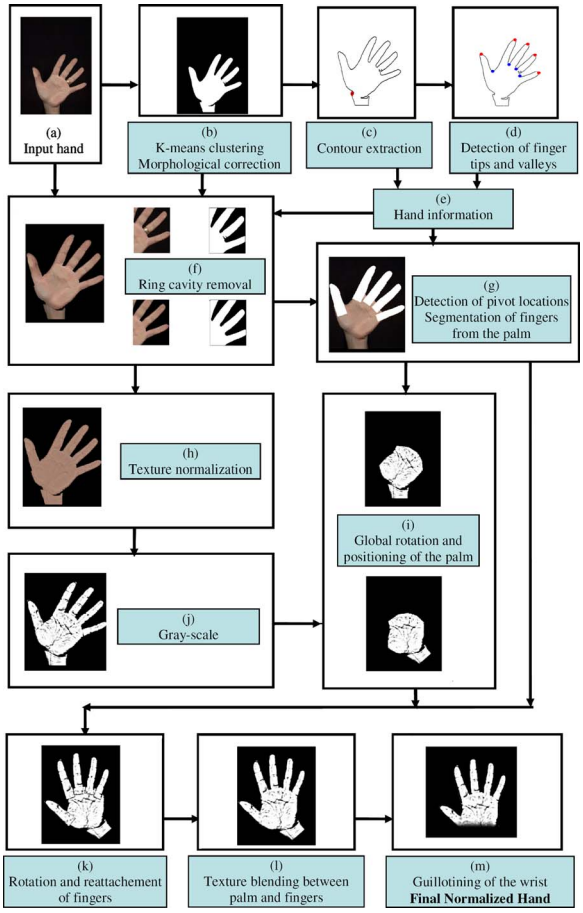

Fig. 12 Block diagram of our hand normalization algorithm with illustrative intermediate outcome images.

We estimate the pivot locations (see Section 2.1), which are the joints between proximal phalanx and the corresponding metacarpal bone, corresponding to the knuckle positions on the reverse side of the hand. The pivots provide robust reference points around which the fingers can be rotated to predetermined directions. The palm texture around these finger joints is corrected for to avoid any artificial texture discontinuity due to rotation.

- *Palmprint extraction*: Palmprint extraction is a byproduct of our normalization algorithm. A rectangular region inside the palm is extracted with the use of pivot locations. The details of this extraction procedure are given in Section 5.3.
- *Wrist guillotining*: The wrist region is guillotined at a certain latitude, which also removes any shadows, cuff artifacts, or foreshortening due to nonflat parts of the wrist. The wrist region is tapered off with a cosinusoidal window that starts from the half-distance point between the pivot line and the wrist line.

Our normalization algorithm can process hands acquired at very different conditions (Fig. 9). The success of the algorithm is 100%, in that all of the hands in our database were successfully normalized. The normalization procedure supplies the proper input format for subsequent feature extraction schemes, from geometrical measures to statistical shape analysis tools, from subspace methods to palmprint-based feature extraction schemes.

The outcome of this algorithm is the normalized hand, which, in turn, can be given as a shape in binary form, as contour information, or as a global hand appearance. The global appearance is referred to as the "handprint." The normalization procedure also includes the extraction of the palmprint region (Fig. 13). In the next section, we briefly describe the features extracted from these "modalities" of the normalized hand.

5 Hand and Palm Features

5.1 *Geometry-Based Hand Features*

Although the focus of our work is holistic hand features, we have also made tests with our own geometrical features for two reasons: first, our hand normalization algorithm provides byproduct key information, such as locations of finger extremities and pivot positions, which can be used to extract geometrical features. Second, the comparative performance of geometric features was never assessed on a database of this size (918 subjects), which is an order of magnitude larger with respect to other test databases in the literature. Our geometrical set consists of 28 features, some of which are illustrated in Fig. 14:

1. five finger lengths computed from the midpoints of the finger baselines to the finger tips. A finger baseline corresponds to the line connecting the two valleys around the corresponding finger.
2. fifteen finger widths measured, respectively for each finger, at the baselines, at one third of the length up, and at two thirds of the length of the fingers.
3. five finger areas.

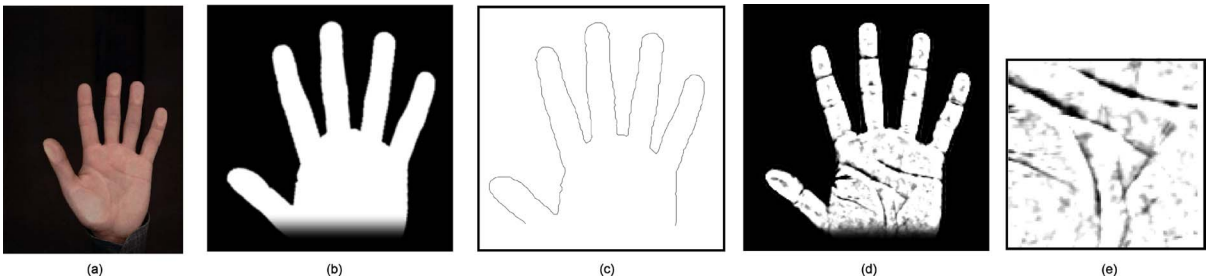

Fig. 13 (a) Original hand; (b) normalized binary hand; (c) hand contour; (d) global hand appearance (handprint); (e) palmprint.

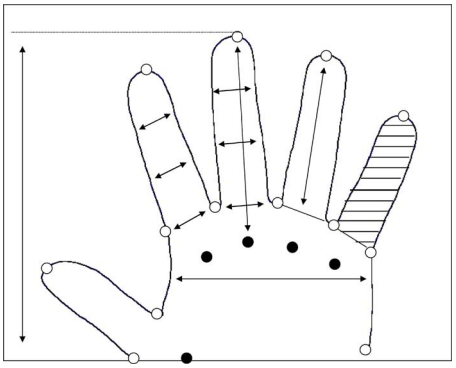

Fig. 14 The geometric measures used for tests on our database.

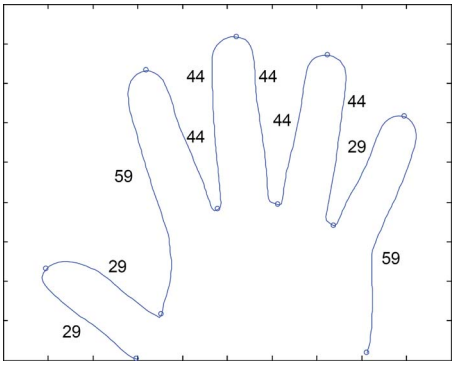

Fig. 15 The number of points between landmark positions in the resampled hand contour.

4. the palm width.
5. the length of the hand.
6. the total area of the hand.

5.2 *Shape-Based Features*

We have considered several features that represent the global shape of the hand. These are extracted from either the binary hand or the hand contour.

5.2.1 *Pixel difference of binary hands*

The pixel difference of binary hands is the sum of the absolute difference of two binary hand images. This simple comparison technique provides a measure of the success of the hand normalization algorithm in mitigating the shape variations due to hand posture and finger orientations. We intend to use it as a baseline against which the gain of the subspace methods can be measured.

5.2.2 *Principal component analysis of binary hands*

Each binary hand is organized in a single lexicographically ordered vector, and then the collection of vectors in the training database is subjected to principal component analysis (PCA). The PCA bases correspond to the eigenvectors of the covariance matrix of the hand vectors. The N-dimensional feature vector of a hand is obtained by projecting it onto the principal N eigenvectors.

5.2.3 *Independent component analysis of binary hands*

We apply the ICA analysis tool on binary hand images to extract and summarize prototypical shape information. ICA assumes that each observed hand image is a mixture of a set of N unknown source signals. Two possible architectures exist for ICA, called ICA1 and ICA2,[72,73] depending on whether one aims for independent basis images or for independent mixing coefficients. In a previous study,[11] we found that the ICA2 architecture yielded superior performance. In the ICA2 architecture, the superposition coefficients are assumed to be independent, but not the basis images. The source and mixing coefficients are then obtained using the FastICA algorithm.[73] We first apply principal component analysis to the training set of binary images to reduce their dimension to N. Then we implement the ICA2 algorithm, which finds a linear transformation that minimizes the statistical dependence between the mixing coefficients.

5.2.4 *Distance between contours*

The contour of the normalized binary hand is another feature set of the hand. The difference between two hand contours is the sum of the absolute difference between the coordinates of the corresponding points. In order to build the correspondences, we utilize 11 landmarks (5 fingertips, 4 finger valleys, and the starting and terminating points of the contours). We uniformly sample the 10 intervals between the successive landmarks, each at a fixed number of samples, as denoted in Fig. 15. In total, hand contours have 435 points.

5.2.5 *Discrete Fourier transform of the contours*

Fourier descriptors are efficient features for shape characterization due to their scale, translation, and rotation invariance, as well as their immunity from small shape perturbations. Fourier descriptors are derived from the discrete Fourier transform (DFT) coefficients of a closed contour that is represented as a periodic complex function. We represent the hand contour as a complex function, where x-coordinates form the real part and y-coordinates the imaginary part. We use the first K DFT coefficients as features, where K varies between 15 and 50, depending on the number of classes (subjects). We do not apply any normalization on the coefficients, since our hand contours are already pose-normalized. The real and imaginary parts of the raw DFT coefficients are concatenated to form a feature vector of size $2K-1$.

5.3 *Palmprint Features*

We utilize the pivot locations extracted in the hand normalization step to localize and scale the palmprint region (Fig. 16). The line connecting the pivots of the index and little fingers constitutes the upper side of the rectangle. The rectangle is extended until it intersects the parallel line passing through the pivot location of the thumb. The region is then resized to a fixed-size image with linear interpolation.

We extract PCA- and ICA-based features from the palmprint image. The PCA-based approach is known as the eigenpalm approach and has been implemented by several authors.[48–51,68] The PCA- and ICA-based feature extraction

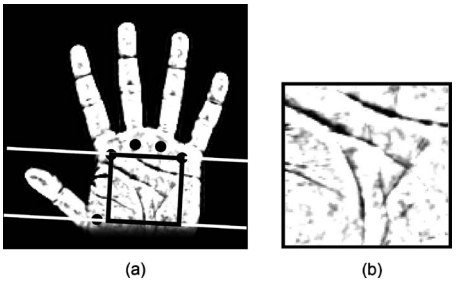

Fig. 16 Extraction of the palmprint region. (a) The rectangular region determined by pivot locations; (b) the extracted palmprint.

procedures are as described in Section 5.2; the only difference is that we form the data vectors from the palm images.

5.4 *Global Hand Appearance*

In order to incorporate the texture and shape information of the hands, researchers have proposed fusion methods at the feature and score levels.[22] These schemes involve separate treatment of each modality, i.e., the shape and palm features are extracted separately and, in general, are of a different nature. For example, Kumar *et al.* fused geometric features representing the shape and the Fourier coefficients extracted from the palm.[22]

In our study, we make use of the "handprint," the outcome of our normalization algorithm, in order to extract features that inherently represent shape and texture jointly. The handprint contains the palm texture, finger creases, and the silhouette of the normalized hand.

Recall that the hand normalization stage outputs a binary hand image, I_{shape}, as well as grayscale textured hand image, $I_{\text{appearance}}$. The gray-level values of the hand texture are normalized to have unit mean and unit variance. Then, a composition of the binary shape image and its textured version is fed to the ICA feature extractor, as illustrated in Fig. 17. The composition of shape and texture components can be adjusted by altering the weighting factor, or texture-to-shape ratio, denoted as α:

$$I = I_{\text{shape}} + \alpha I_{\text{appearance}}, \quad 0 \leq \alpha \leq 1.$$

By reducing the weighting factor, the contribution of the texture component is attenuated. In fact, when it is set to zero, the input to the feature extractor becomes pure shape, i.e., the normalized hand silhouette.

6 Experimental Results

In this section, we report on novel performance results of hand biometry, with and without texture. We give performance figures with respect to various hand features. We address the relative contributions of shape and texture, fusion schemes of right and left hands at various levels, the generalization ability of the ICA-based scheme, the time-lapse issue, and robustness to the resolution of hand images.

Fig. 17 Weighted combination of shape and texture components.

Table 1 The properties of the hand database.

Set	Hand Type	# Subjects	# Samples/Subject	Time Lapse
A	Left	918	3	Short
B	Left and right	800	2×3	Short
C	Left	160	3+2	One month to two years
D	Left and right	100	$2\times3+2\times3$	One month to two years

6.1 *Hand Database*

Our database contains hands from 918 subjects acquired with flatbed scanners within four years. No positioning aids were used. The users laid their hands comfortably on the scanner in any orientation, with the only constraint that their fingers were kept apart. Users were not required to take off their accessories such as rings and watches. All the images were originally scanned at 150 dpi and reduced to 45 dpi via bilinear resizing. None of the users or their images was discarded.

Table 1 gives a summary of the properties of the database. The database is organized in four sets according to the hand type (left and right) and time lapse. Set A contains the left-hand images of 918 subjects, while set B contains ambidextrous recordings, that is, 800 subjects out of a total of 918 have both left- and right-hand images. The subjects in sets C and D form a subset of those of A and B, whose hand images were reacquired after a time lapse varying from two weeks to three years. Figure 18 shows the histogram of the time lapse between two scanning sessions of the subjects in set C. The average time lapse is one year. In set C, only left hands are present, whereas set D contains the time-lapse

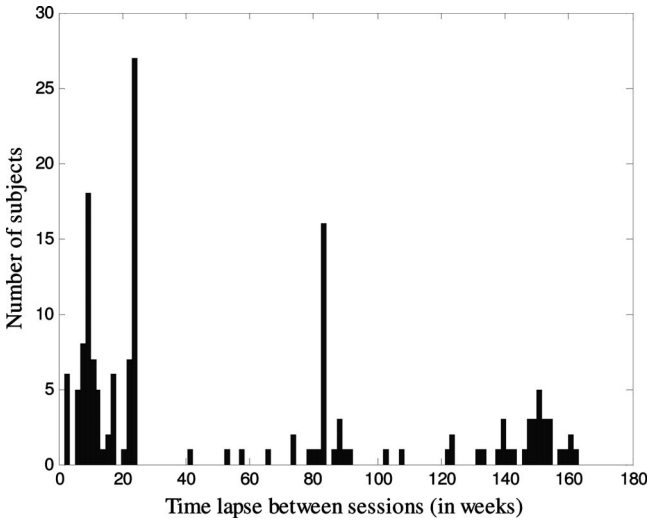

Fig. 18 Histogram of the time lapse between two sessions of the subjects in set C.

Fig. 19 Hand images of six subjects. The first row contains first session hands. The second row contains hand images of the same six subjects acquired after time lapse varying between two weeks and three years.

rescanned left and right hands of 100 subjects. The effect of the time lapse is demonstrated in Fig. 19, where the second row contains the later hand images of the six subjects in the first row.

6.2 *Performance and Feature Types*

In this section, we compare the performance of various feature types. Table 2 gives the rank-1 identification performance with these features under changing population sizes. For each population size, random subsets were drawn from the largest set, i.e., from set A, and the gallery and test images were interchanged, leading to multiple experiments. The average performance of these experiments is reported in Table 2. We considered four different representation types, namely (1) hand contours, (2) shape of the hand silhouette, also called binary hand, (3) palmprint image extracted from a rectangular window on the palm, (4) hand appearance, the hand texture bounded by the hand silhouette shape. A number of conclusions can be drawn from these figures:

- *Raw data versus PCA subspace data*: We see that PCA, when applied to the hand appearance data, brings negligible performance advantage and, for large populations, even causes some small performance loss. Its only advantage is in reducing hand image data by approximately two orders of magnitude. In other words, from the image size (200×200) down to the population size, since we can get at most that many independent columns. It is also noteworthy that ICA always outperforms PCA by 2 to 3 percentage points. This is in contrast to the face literature, where ICA and PCA were reported to have a similar performance.[72]
- *The top-performing feature*: The top-performing feature was found to be ICA (Architecture II) operating on the hand appearance data. This is closely followed by ICA-II features operating on binary shape and DFT coefficients of hand contour data with linear discriminant analysis. The addition of texture information to the ICA scheme (binary versus textured hands) proves especially beneficial for large population sizes.
- *Discriminant analysis*: We have applied LDA (linear discriminant analysis) on geometric measures and on DFT coefficients of the contour and these are the only feature types that benefited from the class information in the enrollment phase. The reasons to use LDA for geometric features were that they were very disparate

Table 2 Identification performance with respect to the feature type and the population size. Enrollment size is 2; only left hands are used.

	Population Size	50	100	200	400	600	918
	Number of Experiments	180	90	60	30	15	3
Shape	Geometric measures (with LDA)	98.36	98.77	98.22	97.79	97.71	97.49
	Point set difference of the contours	98.28	97.49	96.24	94.56	93.83	92.88
	Mean absolute difference of pixel maps of binary hands (EXOR)	98.39	97.90	96.97	96.77	95.53	95.03
	PCA on binary hands	98.44	98.00	97.28	96.10	95.61	95.21
	ICA on binary hands	99.49	99.34	98.99	98.21	98.71	98.69
	DFT on contour (with LDA)	98.41	99.34	99.44	99.38	99.23	99.31
Palm texture	PCA on palm texture	95.31	94.73	93.76	92.82	92.50	91.98
	ICA on palm texture	95.59	95.10	93.88	91.79	93.31	93.83
Appearance	Pixel difference of appearance	99.34	99.29	98.89	98.33	98.23	97.93
	PCA on appearance	99.06	98.73	98.18	97.46	97.19	96.66
	ICA on appearance	**99.73**	**99.74**	**99.52**	**99.40**	**99.44**	**99.42**

in size (areas, lengths, etc.) and LDA contributed to their normalization. With this advantage, geometric measures give fairly good results as compared to other shape-based methods, with the exceptions of the DFT and ICA features.

- *Shape contour versus shape alpha-plane*: We have observed that point set difference of the contours yielded relatively poor identification results. The first reason is that small variations in hand shape have more impact on contour information than on the binary image. Second, the hand contour samples are not in perfect correspondence, since we just apply uniform sampling between the 11 landmarks (5 fingertips, 4 finger valleys, and the first and last points of the contours). In contrast, the binary hand silhouette (shape alpha-plane) consistently yielded better results.
- *DFT coefficients*: DFT coefficients of the contours give a good identification performance, very close to that of the ICA-based method. The main reasons for this high performance are that we apply LDA on the raw DFT coefficients, and LDA reweights these coefficients such that maximum class separation is obtained for the training samples. Furthermore, the Fourier descriptors smooth out the small shape variations on the contour irrelevant to class characteristics and ignore correspondence mismatches among different hands. The high performance yielded by the DFT coefficients show the success of our hand normalization algorithm and strengthens our claim that the shape of the hand contour contains richer information than the geometric measures.
- *Palmprint-based features give the worst results*: We have observed that the varying amount of stretching in the palm from session to session and the contact flattening cause folds on the mass of the palm and displace the palm lines, resulting in misalignment between palm features. Our performance figures are comparable to the state-of-the-art palmprint recognition from low-resolution images. For example, Kumar and Zhang[23] reported a 95.8% classification rate of palmprints with a population of size 100. We have obtained a 95.1% recognition rate on average with 90 different sets consisting of 100 subjects. With increasing populations, the discriminating ability of palmprint features reduces to unacceptable levels. This means that, unless palmprint data are collected with specialized equipment as developed by Zhang *et al.*,[43] these data will have mediocre reliability.

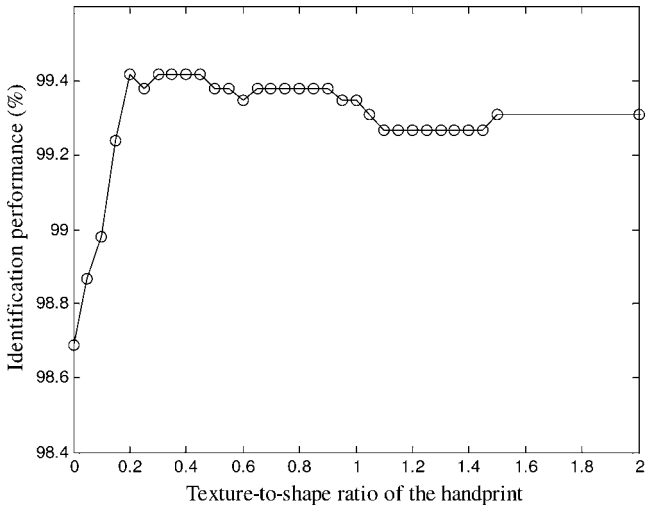

Fig. 20 Identification performance as a function of texture-to-shape ratio α. The population is of size 918 (set A).

6.3 *Contribution of Shape and Texture*

We can control the contribution of the texture relative to the hand silhouette by adjusting a weighting parameter, as explained in Section 5.4. This weighting parameter is the ratio of the gray-level variation of the handprint to the level of the binary hand shape. Figure 20 gives the identification performance with ICA features for varying texture-to-shape ratios α. The database is set A, which contains the left hands of 918 people. ICA-based features are extracted for classification. When we use only binary silhouette, the performance is 98.69%. As we increase the texture-to-shape ratio from 0 to 0.3, the performance increases and reaches its maximum value of 99.42%. We encounter a broad maximum; increasing the texture component beyond α=0.9 degrades the performance slightly, down to 99.27%.

6.4 *Fusion of the Left and Right Hands*

If both right and left hands are measured, several fusion opportunities arise. First, with our precise registration algorithm we can fuse the right and left hands at the data level through averaging them. Notice that a right hand is simply flipped over horizontally, normalized, and summed with its corresponding left hand. The second alternative is fusion at the feature level, where two different ICA vectors are constructed for right and left hands, and then these feature

Table 3 Identification performance with left and right hands and with the fusion of right and left hands. The population is of size 800 (set B). ICA-based features of global hand appearance are used.

	No Fusion		Fusion of Left and Right Hands			
Enrollment Size	Left	Right	Data Fusion	Feature Fusion	Score Fusion (Max Rule)	Score Fusion (Sum Rule)
1	98.00	97.48	99.63	99.65	99.40	99.73
2	99.42	99.13	99.88	99.92	99.92	99.92

Table 4 Identification performance with respect to the size of the training set for building the ICA subspace. The gallery set is of size 918 and contains both seen and unseen subjects during the subspace-building phase.

	Number of Features						
Training Set Size	50	100	200	300	400	500	600
50	95.51						
100	95.85	97.69					
200	96.30	98.16	98.83				
300	96.81	98.39	98.99	99.14			
400	96.70	98.42	98.97	99.16	99.23		
500	96.67	98.65	99.07	99.24	99.27	99.32	
600	96.84	98.69	99.09	99.27	99.31	99.24	99.20
700	96.70	98.73	99.20	99.38	99.31	99.38	99.38
800	96.55	98.69	99.16	99.38	99.42	99.38	99.46
918	96.84	98.69	99.24	99.38	99.42	99.42	99.46

vectors are concatenated. The third alternative is to use fusion at the score level. We have implemented and compared score-level fusion with max and sum rules.

We have conducted experiments on the database of size 800 (set B) using the ICA-based features extracted from global hand appearance. Table 3 gives the identification performances of the single hand versus both hands fused in various styles of data, feature, and score. The main observations are as follows:

- *Data fusion*: When we average normalized gray-level appearances of the right and left hands, the performance improves by 1.63 points, from 98.00 to 99.63 for single enrollment, and by 0.46 points, from 99.42 to 99.88, for double enrollment. Notice that in double enrollment we take the average of four hands.
- However, to be fair, we have to compare equal amounts of data. Thus, when we compare the "single hand and double enrollment" situation with "double hand and single enrollment," the advantage of ambidextrous biometry is much less impressive. The performance differential becomes 0.21 points (cf. 99.63 −99.42). In other words, we can avoid the discomfort of ambidextrous access control simply with multiple enrollments.
- Finally, if subjects have two training samples per hand and are enrolled ambidextrously, the performance climbs to 99.92. This means that only one person in 800 is not recognized. These experiments were conducted in three stages by interchanging the gallery and probe hand images; one out of the three experiments ended up with a 100% recognition rate, and in the other two experiments only one hand was misclassified. The misclassified hand and its normalized version are shown in Figs. 21(a) and 21(c), respectively. Obviously, this is a faulty image where the two fingers are not sufficiently kept apart, as shown in Fig. 21(b).
- Score fusion under the sum rule seems to perform slightly better than score fusion under the max rule or data fusion. Note that for score fusion, left and right hands are considered separately, each having its own subspace.
- Feature fusion also gives slightly better results than data fusion. Feature fusion necessitates separate subspace-building phases for left and right hands, and each hand is separately projected to either the left or right subspace. Then the projections are concatenated and a double-size feature vector is obtained. Thus, feature fusion is computationally more expensive than data fusion.

Despite the improvement of 0.20–0.50 percentage points on a population of size 800 in recognition performance, the employment of both right and left hands in a practice is disputable due to the increased user discomfort.[71] Finally, it

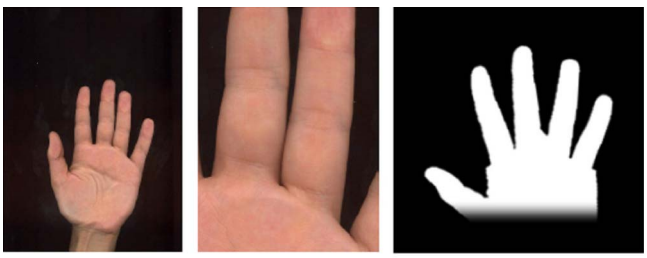

(a) (b) (c)

Fig. 21 (a) The misclassified hand; (b) its zoomed version; (c) its normalized shape.

is conceivable to have a system that accepts both right and left hands. The system must enroll subjects ambidextrously and will operate on the left-hand or right-hand mode according to the placement of the test hand in the device. This choice would be a convenience for right-handed and left-handed people, for people with occasionally injured and bandaged hands, or simply when one of the hands is busy holding other objects.

6.5 *Generalization Ability of the ICA-Based Scheme*

The generalization ability of a subspace-based method is defined as its capability to function with new data, that is, to serve as basis vectors for new data that were not used in the first place to construct the basis set, and it is important for three reasons: first, the subspace-building phase requires memory and computation time; hence, it is undesirable to retrain the system every time a new user is registered to the system. Second, the system should be able to model unseen subjects, especially for verification tasks. Third, the subspace trained in one population should be exploitable for another population. Thus, the ICA basis vectors from one population of subjects should function as the basis set, providing a ready-to-use system for a new application without the necessity of collecting images to build a subspace.

We can classify the subjects into three sets: the training set, the gallery set, and the impostor set. The training set contains images of the subjects that are used to build the subpace, in our case the ICA subspace. The gallery set consists of subjects that are registered to the system and are expected to be identified or verified. These two sets can be identical, totally different, or intersecting. The impostor set is disjoint from the training and gallery sets and consists of unauthorized users that should be rejected by a verification system. We have conducted three different experiments in order to test the generalization ability of our ICA-based recognition system.

6.5.1 *The effect of the training set size*

In the first experiment, the identification performance is calculated on a test set of 918 people (set A), using various ICA subspaces built with training sets of different sizes, each corresponding to a different subset of set A. Hence, the gallery set contains both seen and unseen subjects during construction of the ICA subspace. For example, we use a randomly chosen subset of 200 hands to build the ICA subspace and recognize persons in a set of 918 persons, without the contributions of the 718 remaining subjects for building the ICA basis vectors. Table 4 gives the results of the identification performance under various training set sizes and number of features. Five random combinations of training samples are drawn from the population and the identification experiment is repeated five times for training set sizes of 50 to 500 and the average identification performance is reported. For larger training set sizes, i.e., of 600 to 918, the experiment is carried out for only one combination of training and test samples. The number of features is chosen equal to or less than the training set size since the dimensionality of the ICA subspace is limited by the number of available images. We can make two observations: (1) for a fixed number of features, the performance deterioration with increasing training set size is marginal; (2) the optimal feature size seems to be 300, as there is not much of an improvement for population sizes from 300 up to 918. For example, when we increase the training set size from 300 subjects to the maximum possible size, i.e., 918, and the feature components from 300 to 600, the number of misclassified samples only drops from 8 to 5.

Table 5 Identification performance with respect to the size of the training set for building the ICA subspace. The gallery subjects are chosen from a population apart from the training subjects.

Training Set Size for Building ICA Subspace	Gallery Set Size (Only Unseen Subjects in the ICA Space-Building Phase)	Identification Performance	# Misclassified Images
50	400	96.35	15
100	400	98.45	6
200	400	98.95	4
300	400	99.28	3
400	400	99.42	2
500	400	99.40	2

6.5.2 *Disjoint training and gallery sets*

In the second experiment, the training and the gallery sets are totally disjoint. This is the case when the system is trained on a given population and then exported to another platform where totally different subjects use the system. The gallery set consists of 400 subjects. The identification performance increases incrementally after the training set size reaches 100 (Table 5). For all training set sizes, we have drawn five random combinations of training and gallery subjects and averaged the identification performances obtained from the five experiments. The results in Table 5 indicate that this biometric system is completely generalizable, in view of the uncompromising high identification performance.

Table 6 Verification performance with respect to the size of the training set for building the ICA subspace. The gallery and impostor subjects are chosen from a population apart from the training subjects.

Training Set Size for Building ICA Subspace	Gallery Set Size (Unseen Subjects in the ICA Space-Building Phase)	Impostor Set Size (Unseen Subjects in the ICA Space-Building Phase)	Equal Error Rate (%)
50	400	100	1.24
100	400	100	0.66
200	400	100	0.40
300	400	100	0.27
400	400	100	0.21

Table 7 Identification performance with respect to time lapse. ICA-based features of global hand appearance are used.

Training Set Size for Building ICA Subspace	Number of Users in the Gallery (3 enrollments/user)	Number of Test Subjects (2 samples/user)	Identification Performance (%)	# Misclassified Images
160	160	160	98.75	4
300	160	160	99.38	2
918	160	160	100	0
918	918	160	99.06	3

6.5.3 *Verification and impostor rejection*

In the third experiment, we simulate a verification scenario, where the gallery set and impostor set consist of 400 and 100 subjects, respectively. We have 400 genuine-to-genuine and 100×400 impostor-to-genuine comparisons. None of the gallery and impostor subjects has been seen at the subspace-building phase. The system is trained with different sizes of populations, as in the second experiment above. Table 6 gives the equal error rates. These error rates are averaged over fivefold experiments where combinations of training, genuine, and impostor subjects are selected randomly. We observe that after reaching a training set size of 100, the improvement is not significant. Figure 22 shows the receiver operating characteristics of the system; the ROC curves of systems trained with 200, 300, and 400 subjects are hardly differentiable. We can conclude that the system has good impostor rejection performance.

These three experiments demonstrate that our ICA-based hand recognition scheme can adequately model hands that were unseen during the model-building phase. The trained subsets can be imported to other populations with identification rates higher than 99% and equal error rates lower than 0.4%.

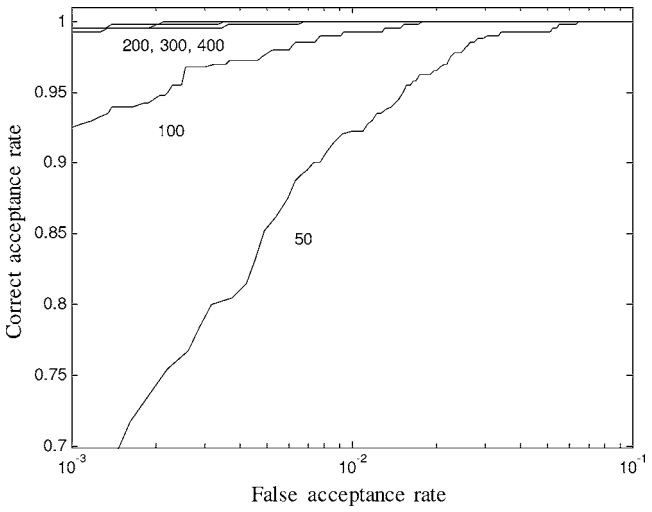

Fig. 22 ROC curves with respect to the size of the training set for building the ICA subspace.

6.6 *Performance Under Time Lapse*

Robustness with respect to time lapse is the most critical issue of a biometry-based identification system. Table 7 gives the identification rates obtained on a test set of 160 subjects (set C). Hence, we conducted experiments with time-lapse images, which were acquired after a period ranging from two weeks to three years (Figs. 18 and 19). In the experiments, we varied the population size of the training set for building the ICA subspace and only "old images" were used. When we use only the old images of 160 subjects for training, we end up with 4 misclassified cases within recent test hands of these subjects. As the number of training images increases, the dimensionality of the subspace, hence the number of features, increases, and we achieve 100% recognition rate. The last experiment in Table 7 corresponds to the case where new images of 160 people are compared with the full gallery of 918 subjects, i.e., 918 classes exist. Even in this difficult setup, the identification performance is 99.06%.

Since there are no standard hand databases and protocols, it is difficult to evaluate the relative success of alternate works on different databases. However, in Table 8, we give the identification and verification results reported by several authors. In this table, we also indicate the key parameters of each experiment. All experiments are performed on databases consisting of 100 subjects since this was the population size common to the other studies in the literature in Table 8. We have conducted our experiments on set D, with the ICA-based features extracted from the global hand appearance. Each subject has three test images. The verification results are obtained using an impostor set

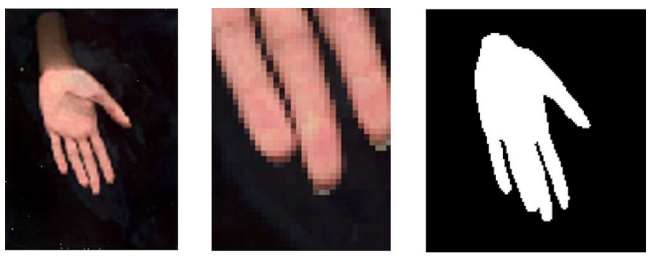

Fig. 23 (a) Sample hand image at 15 dpi; (b) zoomed hand image; (c) result of segmentation.

Table 8 Comparison of our method with previous work.

	Features	Enrollment Size	Time Lapse	Hand Type	Performance
Kumar *et al.*, 2006[22]	Magnitude and direction of palm lines + geometric measures of the hand	5	Three months	Left	Verification: 3.74% FAR, 1.91% FRR
Kumar and Zhang, 2006[23]	DCT coefficients of palm image + geometric measures of the hand	5	Three months	Left	Identification: 98%
Kumar and Zhang, 2005[48]	Fusion of multiple features from the palm (Gabor features, Line features, PCA features)	5	Three months	Right	Verification: 0.08% FAR, 4.6% FRR
Shang *et al.*, 2006[57]	ICA (FastICA) on the palm	3	Two months	Right	Identification: 98.67%
Our method	ICA2 on the global hand appearance	3	Two weeks to three years	Left	Identification: 99.33%, verification: 1% EER
Our method	ICA2 on the global hand appearance	3	Two weeks to three years	Right	Identification: 98%, verification: 1.16% EER
Our method	ICA2 on the global hand appearance with fusion of left and right hands	2×3	Two weeks to three years	Left and Right	Identification: 99.67%, verification: 0.33% EER

of 100 subjects with three hand images for each, leading to 300 genuine-to-genuine comparisons and 300×100 impostor-to-genuine comparisons. Although the performance figures in Table 8 were obtained with different hand databases, we believe that they nevertheless give an idea of the success of the hand appearance-based algorithm.

6.7 *Effect of Resolution on the Performance*

We have tested our normalization algorithm and ICA-based feature extraction scheme under various image resolutions. All other experiments in this work were performed with 45-dpi resolution, and the resulting normalized images were of size 200×200. We reduced the resolution to 30 and 15 dpi via linear interpolation and conducted identification experiments on set A (population 918). The rates of success for normalization and identification are given separately in Table 9.

When some images are downsampled to a lower resolution, fingers that are close to each other tend to merge, which makes the hand normalization impossible. There were two such hand images with resolution 30 dpi and six images with resolution 15 dpi, and they were discarded from the identification experiments. A sample case is illustrated in Fig. 23.

This analysis shows that our normalization algorithm can work with very low-resolution images and the identification performance remains above 96%, even at 15 dpi.

7 Conclusions

Our detailed investigation of the various aspects of hand biometry reveals that person identification and verification can be successfully implemented with hand imaging devices. Our major conclusions on the device technology and subject set list as follows:

Device: (1) proper hand registration with finger reorientations is critical for high-performance operation; (2) the algorithm can accept input from imaging devices with as

Table 9 Identification performance with respect to resolution. The population is of size 918 (set A). ICA-based features of global hand appearance are used.

	45 dpi	30 dpi	15 dpi
Success of normalization (%)	100	99.79	99.35
Identification performance (%)	99.42	99.02	96.24

low a resolution as 30 dpi and hands containing various accessories; (3) the hand normalization system can work with a wide range of acquisition devices such as scanners and low-resolution cameras.

Subject set: (4) hand biometric access control can be applied very reliably to populations from hundreds to a thousand subjects; (5) the hand biometric system trained on a given population can be exported to operate on a partially or totally differing population; (6) the algorithm does not suffer noticeable performance loss over time lapses from several months to a year.

The work is continuing to assess its complementary role in a multimodal setting with larger populations.

References

1. R. P. Miller, "Finger dimension comparison identification system," U.S. Patent No. 3576538 (1971).
2. R. H. Ernst, "Hand ID system," U.S. Patent No. 3576537 (1971).
3. I. H. Jacoby, A. J. Giordano, and W. H. Fioretti, "Personnel identification apparatus," U.S. Patent No. 3648240 (1972).
4. D. P. Sidlauskas, "3D hand profile identification apparatus," U.S. Patent No. 4736203 (1988).
5. M. Gunther, "Device for identifying individual people by utilizing the geometry of their hands," Eur. Patent No. DE10113929 (2002).
6. B. Miller, "Vital signs of identity," *IEEE Spectrum* **32**(2), 22–30 (1994).
7. R. L. Zunkel, "Hand geometry based verification," in *Biometrics*, A. Jain, R. Bolle, and S. Pankanti, Eds., Kluwer Academic Publishers, New York, pp. 87–101 (1999).
8. J. Holmes, L. Wright, and R. Maxwell, "A performance evaluation of biometric identification devices," Sandia National Laboratories (1991).
9. A. K. Jain, A. Ross, and S. Prabhakar, "An introduction to biometric recognition," *IEEE Trans. Circuits Syst. Video Technol.* **14**, 4–20 (2004).
10. E. Kukula and S. Elliott, "Implementation of hand geometry: An analysis of user perspectives and system performance," *IEEE Aerosp. Electron. Syst. Mag.* **21**(3), 3–9 (2006).
11. E. Konukoğlu, E. Yörük, J. Darbon, and B. Sankur, "Shape-based hand recognition," *IEEE Trans. Image Process.* **15**(7), 1803–1815 (2006).
12. E. Yörük, H. Dutagaci, and B. Sankur, "Hand biometrics," *Image Vis. Comput.* **24**(5), 483–497 (2006).
13. V. I. Pavlovic, R. Sharma, and T. S. Huang, "Visual interpretation of hand gestures for human-computer interaction: A review," *IEEE Trans. Pattern Anal. Mach. Intell.* **19**(7), 677–695 (1997).
14. J. J. Kuch and T. S. Huang, "Vision based hand modeling and tracking," in *Proc. Int. Conf. Computer Vision*, Cambridge, MA (1995).
15. J. Lin, Y. Wu, and T. S. Huang, "Modeling the constraints of human hand motion," in *Proc. Workshop on Human Motion (HUMO'00)*, pp. 121–126 (2000).
16. A. K. Jain, A. Ross, and S. Pankanti, "A prototype hand geometry-based verification system," in *Proc. 2nd Int. Conf. Audio and Video-Based Biometric Person Authentication (AVBPA)*, pp. 166–171 (1999).
17. R. Sanchez-Reillo, C. Sanchez-Avila, and A. Gonzalez-Marcos, "Biometric identification through hand geometry measurements," *IEEE Trans. Pattern Anal. Mach. Intell.* **22**(10), 1168–1171 (2000).
18. A. L. N. Wong and P. Shi, "Peg-free hand geometry recognition using hierarchical geometry and shape matching," in *Proc. IAPR Workshop on Machine Vision Applications*, pp. 281–284 (2002).
19. Y. Bulatov, S. Jambawalikar, P. Kumar, and S. Sethia, "Hand recognition using geometric classifiers," in *Proc. DIMACS Workshop on Computational Geometry*, pp. 14–15 (2002).
20. C. Oden, A. Ercil, and B. Buke, "Combining implicit polynomials and geometric features for hand recognition," *Pattern Recogn. Lett.* **24**, 2145–2152 (2003).
21. A. Kumar, C. M. Wong, H. C. Shen, and A. K. Jain, "Personal verification using palmprint and hand geometry biometric," in *Proc. 4th Int. Conf. Audio- and Video-Based Biometric Person Authentication (AVBPA)*, Guildford, UK (2003).
22. A. Kumar, C. M. Wong, H. C. Shen, and A. K. Jain, "Personal authentication using hand images," *Pattern Recogn. Lett.* **27**, 1478–1486 (2006).
23. A. Kumar and D. Zhang, "Personal recognition using hand shape and texture," *IEEE Trans. Image Process.* **15**(8), 2454–2461 (2006).
24. A. K. Jain and N. Duta, "Deformable matching of hand shapes for verification," in *Proc. ICIP*, pp. 857–861 (1999).
25. T. F. Cootes, G. J. Edwards, and C. J. Taylor, "Active appearance models," *IEEE Trans. Pattern Anal. Mach. Intell.* **23**, 681–685 (2001).
26. M. Bober, "MPEG-7 visual shape descriptors," *IEEE Trans. Circuits Syst. Video Technol.* **11**, 716–719 (2001).
27. T. Funkhouser, P. Min, M. Kazhdan, J. Chen, A. Halderman, and D. Dobkin, "A search engine for 3D models," *ACM Trans. Graphics* **22**(1), 83-105 (2003).
28. http://www.rcgravel.com/palm_print_identification.htm.
29. W. Shu and D. Zhang, "Palmprint verification: An implementation of biometric technology," in *Proc. 14th Int. Conf. Pattern Recog.*, 1, 219–221 (1998).
30. D. Zhang and W. Shu, "Two novel characteristics in palmprint verification: Datum point invariance and line feature matching," *Pattern Recogn.* **32**(4), 691–702 (1999).
31. N. Duta, A. K. Jain, and K. V. Mardia, "Matching of palmprints," *Pattern Recogn. Lett.* **23**, 477–485 (2002).
32. L. Liu and D. Zhang, "Palm-line detection," in *Proc. IEEE Int. Conf. Image Processing* 3, 269–272 (2005).
33. X. Wu, K. Wang, and D. Zhang, "A novel approach of palm-line extraction," in *Proc. 3rd Int. Conf. Image and Graphics*, pp. 230–233 (2004).
34. J. You, W. Li, and D. Zhang, "Hierarchical palmprint identification via multiple feature extraction," *Pattern Recogn.* **35**, 847–859 (2002).
35. K. I. Laws, "Texture energy measures," in *Proc. Image Understanding Workshop* (1979).
36. J. Chen, C. Zhang, and G. Rong, "Palmprint recognition using crease," in *Proc. Int. Conf. Image Process*, pp. 234–237 (2001).
37. J. Funada, N. Ohta, M. Mizoguchi, T. Temma, K. Nakanishi, A. Murai, T. Sugiuchi, T. Wakabayashi, and Y. Yamada, "Feature extraction method for palmprint considering elimination of creases," in *Proc. 14th Int. Conf. Patt. Recog.*, pp. 1849–1854 (1998).
38. X. Wu, K. Wang, and D. Zhang, "Fuzzy directional energy element based palmprint identification," in *Proc. ICPR-2002*, pp. 95–98 (2002).
39. X. Wu, K. Wang, and D. Zhang, "Palmprint recognition using directional line energy feature," in *Proc. ICPR-2004* 4, 475–478 (2004).
40. C. C. Han, H. L. Cheng, C. L. Lin, and K. C. Fan, "Personal authentication using palm print features," *Pattern Recogn.* **36**, 371–381 (2003).
41. F. Li, M. K. H. Leung, and X. Yu, "Palmprint identification using Hausdorff distance," in *Proc. IEEE Int. Workshop on Biomedical Circuits and Systems* (2004).
42. W. K. Kong, D. Zhang, and W. Li, "Palmprint feature extraction using 2-D Gabor filters," *Pattern Recogn.* **36**(10), 2339–2347 (2003).
43. D. Zhang, W. K. Kong, J. You, and M. Wong, "Biometrics—Online palmprint identification," *IEEE Trans. Pattern Anal. Mach. Intell.* **25**(9), 1041–1050 (2003).
44. W. K. Kong and D. Zhang, "Competitive coding scheme for palmprint verification," in *Proc. 17th ICPR* 1, 520–523 (2004).
45. A. Kong, D. Zhang, and M. Kamel, "Palmprint identification using feature-level fusion," *Pattern Recogn.* **39**, 478–487 (2006).
46. W. Li, D. Zhang, and Z. Xu, "Palmprint identification by Fourier transform," *Int. J. Pattern Recognit. Artif. Intell.* **16**(4), 417–432 (2002).
47. A. Kumar and H. C. Shen, "Palmprint identification using PalmCodes," in *Proc. 3rd Int. Conf. Image & Graphics*, pp. 258–261 (2004).
48. A. Kumar and D. Zhang, "Personal authentication using multiple palmprint representation," *Pattern Recogn.* **38**, 1695–1704 (2005).
49. G. Lu, D. Zhang, and K. Wang, "Palmprint recognition using Eigenpalm features," *Pattern Recogn. Lett.* **24**(9–10), 1463–1467 (2003).
50. T. Connie, A. T. B. Jin, M. G. K. Ong, and D. N. C. Ling, "An automated palmprint recognition system," *Image Vis. Comput.* **23**, 501–515 (2005).
51. W. Jiang, J. Tao, and L. Wang, "A novel palmprint recognition algorithm based on PCA & FLD," in *Proc. Int. Conf. Digital Telecommunications, ICDT '06* (2006).
52. Y. H. Pang, T. Connie, A. Jin, and D. Ling, "Palmprint authentication with Zernike moment invariants," in *Proc. 3rd IEEE Int. Symp. Signal Process. Information Technology, ISSPIT*, pp. 199–202 (2003).
53. Q. Dai, N. Bi, D. Huang, D. Zhang, and F. Li, "M-band wavelets application to palmprint recognition based on texture features," in *Proc. Int. Conf. Image Processing, ICIP '04* 2, 893–896 (2004).
54. L. Zhang and D. Zhang, "Characterization of palmprints by wavelet signatures via directional context modeling," *IEEE Trans. Syst., Man, Cybern., Part B: Cybern.* **34**(3), 1335–1347 (2004).
55. C. C. Han, "A hand-based personal authentication using a coarse-to-fine strategy," *Image Vis. Comput.* **22**(11), 909–918 (2004).
56. G. M. Lu, K. Q. Wang, and D. Zhang, "Wavelet based independent component analysis for palmprint identification," in *Proc. Int. Conf. Machine Learning and Cybernetics* 6, 3547–3550 (2004).
57. L. Shang, D. S. Huang, J. X. Du, and C. H. Zheng, "Palmprint recognition using FastICA algorithm and radial basis probabilistic neural network," *Neurocomputing* **69**, 1782–1786 (2006).
58. P. Hennings and B. V. K. Vijaya Kumar, "Palmprint recognition using correlation filter classifiers," *Conference Record 38th Asilomar Con-*

ference on Signals, Systems and Computers **1**, 567–571 (2004).
59. C. Poon, D. C. M. Wong, and H. C. Shen, "A new method in locating and segmenting palmprint into region-of-interest," in *Proc. 17th Int. Conf. Patt. Recog., ICPR 2004* 4, 533–536 (2004).
60. J. You, A. W. K. Kong, D. Zhang, and K. H. Cheung, "On hierarchical palmprint coding with multiple features for personal identification in large databases," *IEEE Trans. Circuits Syst. Video Technol.* **14**(2), 234–243 (2004).
61. W. Li, J. You, and D. Zhang, "Texture-based palmprint retrieval using a layered search scheme for personal identification," *IEEE Trans. Multimedia* **7**(5), 891–898 (2005).
62. J. S. Noh and K. H. Rhee, "Palmprint identification algorithm using Hu invariant moments and Otsu binarization," in *Proc. 4th Ann. ACIS, Int. Conf. Computer and Information Science*, pp. 94–99 (2005).
63. W. Xiong, K. A. Toh, W. Y. Yau, and X. Jiang, "Model-guided deformable hand shape recognition without positioning aids," *Pattern Recogn.* **38**, 1651–1664 (2005).
64. C. L. Su, "Original finger image extraction by morphological technique and finger image comparisons for persons' identification," *J. Intell. Robotic Syst.* **45**, 1–14 (2006).
65. D. Keren, "Using symbolic computation to find algebraic invariants," *IEEE Trans. Pattern Anal. Mach. Intell.* **16**(11), 1143–1149 (1994).
66. G. Fouquier, L. Likforman, J. Darbon, and B. Sankur, "The BIOSECURE geometry-based system for hand modality," in *Proc. IEEE Int. Conf. Acoustic, Speech and Signal Processing (ICASSP)* (2007).
67. D. G. Joshi, Y. V. Rao, S. Kar, and V. Kumar, "Computer vision based approach to personal identification using finger crease pattern," *Pattern Recogn.* **31**(1), 15–22 (1998).
68. S. Ribaric and I. Fratric, "A biometric identification system based on eigenpalm and eigenfinger features," *IEEE Trans. Pattern Anal. Mach. Intell.* **27**(11), 1698–1709 (2005).
69. S. Ribaric and I. Fratric, "An online biometric authentication system based on eigenfingers and finger-geometry," in *Proc. 13th Euro. Signal Processing Conference*, Antalya, Turkey (2005).
70. M. Wong, D. Zhang, W. Kong, and G. Lu, "Real-time palmprint acquisition system design," *IEE Proc. Vision Image Signal Process.* **152**(5), 527–534 (2005).
71. A. Kumar and D. Zhang, "Integrating shape and texture for hand verification," in *Proc. 3rd Int. Conf. Image and Graphics*, pp. 222–225 (2004).
72. B. A. Draper, K. Baek, M. S. Bartlett, and J. R. Beveridge, "Recognizing faces with PCA and ICA," *Comput. Vis. Image Underst.* **91**, 115–137 (2003).
73. A. Hyvarinen and E. Oja, "Independent component analysis: Algorithms and applications," *Neural Networks* **13**, 411–430 (2000).

Biographies and photographs of the authors not available.